Electrochemistry of uranium in molten LiF-CaF2

Christophe Nourry, Pavel Soucek, Laurent Massot, Rikard Malmbeck, Pierre Chamelot, Jean-Paul Glatz

Electrochemistry of uranium in molten $LiF–CaF_2$

C. Nourry [a,*], P. Souček [a], L. Massot [b], R. Malmbeck [a], P. Chamelot [b], J.-P. Glatz [a]

[a] European Commission, JRC, Institute for Transuranium Elements, Postfach 2340, 76125 Karlsruhe, Germany
[b] Laboratoire de Génie Chimique (LGC), Département Procédés Electrochimiques, CNRS-UMR 5503, Université de Toulouse III – Paul Sabatier, 31062 Toulouse cedex 9, France

A B S T R A C T

This article is focused on the electrochemical behaviour of U ions in molten $LiF–CaF_2$ (79–21 wt.%) eutectic. On a W electrode, U(III) is reduced in one step to U metal and U(III) can be also oxidised to U(IV). Both systems were studied by cyclic and square wave voltammetry. Reversibility of both systems for both techniques was verified and number of exchanged electrons was determined, as well as diffusion coefficients for U(III) and U(IV). The results are in a good agreement with previous studies. On a Ni electrode, the depolarisation effect due to intermetallic compounds formation was observed. Electrorefining of U metal in a melt containing U and Gd ions was carried out using a reactive Ni electrode with promising results.

1. Introduction

The present management of spent nuclear fuel is based on direct disposal or single recycling of U and Pu, whereas a strategy known as "Partitioning and Transmutation" (P&T) is being developed in several countries for recovery and separate processing of actinides [1]. The apparent advantages of this approach are a decrease in the volume and radiotoxicity of the final wastes, enhancing the safety of a final repository and of an efficient use of resources.

In this context, pyrochemical processes are one of the routes explored as a promising alternative/complement to the hydrometallurgical methods for recovery and recycling of actinides. Pyrochemical techniques rely on dissolution of the fuel in inorganic compounds, which have high radiation and thermal stability. Shorter cooling times would therefore be required for the fuel before reprocessing, allowing faster and a more compact back-end of the fuel cycle.

It has already been proven that molten chloride media are suitable for dissolution and pyrochemical processing of metallic or oxide fuels [2–5]. However, the inherent high neutron capture of chloride ions excludes the use of molten chlorides in Molten Salt Reactor technology, where molten salts are used as fuel and primary coolant. In this case, fluoride salt media will be more appropriate. Studying properties of actinides in molten fluoride salts is therefore especially important for the understanding of an electrochemical technique for processing of Molten Salt Reactor fuel. It seems very advantageous to recover actinides on some reactive electrode material, as shown, e.g. during development of an electrorefining process for nuclear fuel treatment using molten chloride media. Due to the very demanding working conditions (higher melting point, corrosion, oxide dissolution...), molten fluorides and properties of actinides in those media have not been extensively investigated. In fact only a limited number of studies has been published about electrochemistry of actinides in molten fluorides [6–12].

In the first part of this work, the electrochemical behaviour of U(III) and U(IV) are investigated in $LiF–CaF_2$ eutectic mixture (79–21 wt.%). Previously, the authors have already investigated U(III) in $LiF–CaF_2$ [7] and U(IV) in LiF–NaF [7] or in $LiF–BeF_2–ZrF_4$ [9] melts. The second part is focused on the U recovery on a Ni electrode in a salt containing U and Gd ions. This technique, is close to the technique developed in molten chloride [2,3] based on extraction of actinides on a reactive aluminium cathode. The successful selective reduction of U is a first step for the clean-up of spent fuel from actinides in molten fluoride media.

2. Experimental

2.1. Electrochemical experiments

All the electrochemical experiments and melt preparations were done in a glove box under pure argon atmosphere (<5 ppm of oxygen and moisture). Electrochemical experiments and electrodeposition runs were carried out with a three-electrode set-up connected to a PAR 273 potentiostat using CorrWare2 electrochemical software. A Pt wire immersed in the salt was used as a quasi-reference or comparison electrode (RE), based on the $Pt/PtO_x/O^{2-}$ red-ox system [13]. For analytical experiments, working

* Corresponding author. Tel.: +49 7247 951863; fax: +49 7247 95199124.
E-mail address: Christophe.Nourry@ec.europa.eu (C. Nourry).

http://dx.doi.org/10.1016/j.jnucmat.2012.06.028

electrodes (WE) were made of 1 mm diameter W or Ni wire and the counter electrode (CE) was a Mo wire bent into the shape of a spiral. For the electrorefining, a nickel plate (0.5 cm^2) was used as the cathode and a tantalum basket filled with uranium metal (ITU stock, very high purity) served as the anode.

2.2. Preparation of the melt

Boron nitride (HP grade) was selected as a material for the crucible. Pure LiF and CaF_2 (Alfa Aesar, 99.99% ultra dry, packed under argon) were used for the solvent preparation. The eutectic LiF–CaF_2 (79–21 mol.%) was prepared in the glove box by mixing of the pure chemicals with no additional treatment. U ions were produced by chemical oxidation of metallic uranium by bismuth ions. The melts were prepared according to Eqs. (1) and (2) respectively with an excess of Bi or with an excess of U, leading to the formation of U(IV) or U(III):

$$4Bi^{3+} + 3U = 3U^{4+} + 4Bi \quad (1)$$

$$Bi^{3+} + U = U^{3+} + Bi \quad (2)$$

Theses two melts were prepared for the analysis of the U(IV)/U(III) and U(III)/U(0) systems, respectively. Bi^{3+} was introduced into the melt as BiF_3 (Alfa Aesar 99.999%) and a Bi pool was at the bottom of the crucible and so recovered the metallic Bi formed, as shown in Fig. 1. The conditions used for the melts preparation are summarised in Table 1.

2.3. Analytical techniques

The U concentration in the bath was followed by ICP–MS analysis of the salt samples (about 30 mg) taken during the experiment. The samples were dissolved in 4 ml of HCl (8 M) heated at 80 °C and diluted with 1 M HNO_3 for the measurements. The initial concentrations were 2 and 1.5 wt.% (U metal) for U(III) and U(IV) melts, that is 8.7×10^{-2} mol/kg and 6.5×10^{-2} mol/kg respectively. After the electrorefining the nickel electrode was embedded, cut and the cross-section polished and then analysed with SEM–EDS on a Philips XL40 SEM.

3. Electrochemical analysis of the U system

A comparison of cyclic voltammograms plotted in the pure solvent (thin curve) and in the melt containing U ions (thick curve) is shown in Fig. 2.

After addition of U ions to the melt, two electrochemical systems were observed:

- Soluble–soluble system at a potential of −0.5 V/ref (B).
- Solid phase formation system (sharp reduction and re-oxidation peaks) at a potential of −1.1 V/ref (A).

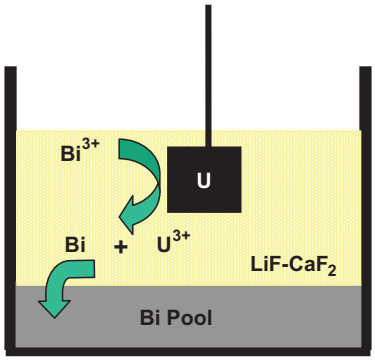

Fig. 1. Scheme of the set-up used for the melt preparation.

Table 1
Preparatory conditions for the two melts.

$m_{LiFCaF2}$ (g)	m_{BiF3} (g)	m_{Uplate} (g)	Reaction time	Colour of the salt
30.00	1.532	1.045	~16 h	Green (U(IV))
29.83	0.905	0.904	~9 h	Purple/red (U(III))

3.1. Reversibility of the system

Cyclic voltammetry and square wave voltammetry were used in this work and the reversibility of both systems was checked for those two techniques at different scan rates and frequencies.

3.1.1. Cyclic voltammetry

A system can be considered reversible if the peak intensity I_p depends linearly on the square root of the scan rate v and if the difference $\Delta E_p = E_{pa} - E_{pc} \sim \frac{2.3RT}{nF}$ [V], where E_{pa} and E_{pc} are the anodic and cathodic peak potential, respectively [14]. The dependency of I_p on $v^{1/2}$ is shown in Fig. 3 for both systems.

The numbers of exchanged electrons are supposed to be 3 and 1 for the studied systems A and B, respectively (cf 3.2). The theoretical values of $\frac{2.3RT}{nF}$ are 0.072 V and 0.216 V, which agree very well with the graphically measured values of ΔE_p, 0.080 V and 0.205 V, respectively. Therefore, both systems were considered as reversible for the studied scan rates.

3.1.2. Square-wave voltammetry

A typical square wave voltammogram of the system is show in Fig. 4.

Both systems observed by cyclic voltammetry (A and B) were also detected on the square-wave voltammogram. The potential difference was caused by a shift of the Pt comparison electrode potential indeed, the comparison potential is higly influenced by O^{2-} concentration. This concentration, is very low during the experiment but may slightly change after electrolysis or immersion of new electrode in the melt. Similarly to the cyclic voltammetry, reversibility of electrochemical systems for square wave voltammetry is evaluated by measuring of the peak intensities I_p versus square root of frequencies f. The dependency of I_p on $f^{1/2}$ is shown in Fig. 5 for both systems. This dependency was linear in the 9–36 Hz range, showing reversibility of both systems for these frequencies [15,16]. For higher frequencies, the system is quasi-reversible.

3.2. Number of exchanged electrons

The number of exchanged electrons was calculated using square wave voltammetry technique according to Eq. (3), which is valid for reversible systems [15–17].

$$W_{1/2} = 3.52\frac{RT}{nF} \quad (3)$$

$W_{1/2}$ is the half width of the peak (V), R is the ideal gas constant (J mol^{-1} K^{-1}), T is the absolute temperature (K), n is the number of exchanged electrons and F is the Faraday constant (C mol^{-1}). Calculations were done with square wave voltammograms plotted at 9 Hz. For the soluble–soluble system, it was possible to directly apply the Eq. (3). However, in case of the second system, the signal was modified due to the currentless nucleation phase of the metal deposition [7]. The peak was deconvoluted into two half Gaussian curves. The more negative one, uninfluenced by nucleation, was

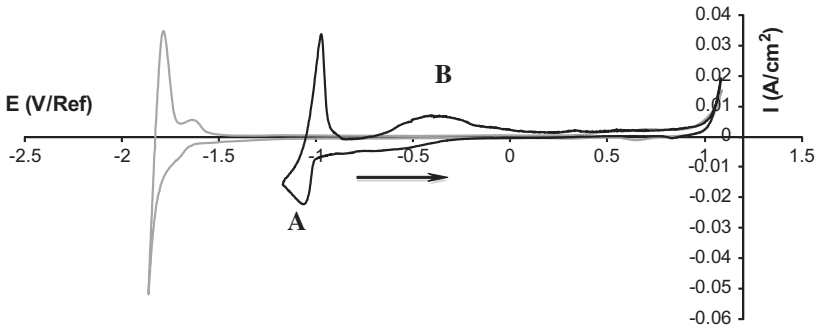

Fig. 2. Comparison of cyclic voltammograms plotted in LiF–CaF_2 (grey curve) and in LiF–CaF_2–UF_3 (8.7 10^{-5} mol/kg) (black curve) at 1083 K; WE: W, CE: Mo, RE: Pt; v = 100 mV/s.

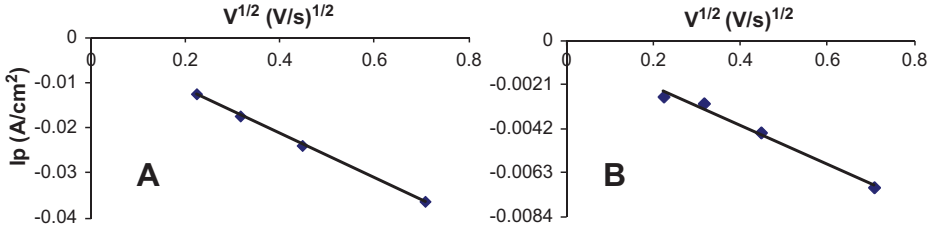

Fig. 3. Dependency of the peak intensity (I_p) of peaks $A + B$ in Fig. 2 of the U systems versus the square root of sweep rate (50, 100, 200 and 500 mV/s).

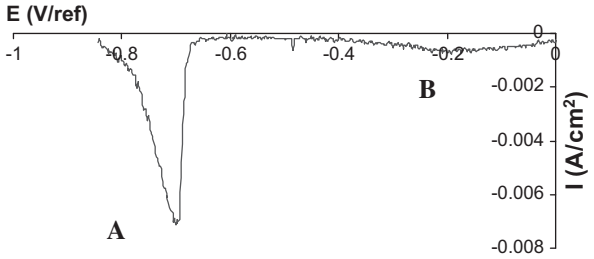

Fig. 4. Square wave voltammogram of the LiF–CaF_2–UF_3 (8.7×10^{-5} mol/kg) system at 1090 K; WE: W, CE: Mo, RE: Pt; f = 9 Hz.

extrapolated to form the complete Gaussian curve. Fig. 6 shows the original experimental curve and the deconvoluted signal.

According to Eq. (3), the number of exchanged electrons is 2.9 ± 0.2 and 1.0 ± 0.1 electrons for the systems A and B, respectively. Thus the reduction of U(IV) to U metal in molten LiF–CaF_2 proceeds in two steps. The first step involves one electron and leads to formation of U(III), the second step involves three electrons and U metal is formed according to Eqs. (4) and (5), respectively:

$$U(IV) + e^- \rightarrow U(III) \quad (4)$$

$$U(III) + 3e^- \rightarrow U(0) \quad (5)$$

3.3. Determination of the diffusion coefficient

Diffusion coefficients were calculated on the basis of cyclic voltammetry, applying the Randles–Sevcik equation (Eq. (6)) for the soluble U(IV)–U(III) system and the Berzins–Delahaye [18,19] equation (Eq. (7)) for the U(III)–U(0) system with an insoluble product:

$$i_p = 0.446(nF)^{3/2}(RT)^{-1/2}C(Dv)^{1/2} \quad (6)$$

$$i_p = 0.61(nF)^{3/2}(RT)^{-1/2}C(Dv)^{1/2} \quad (7)$$

i_p is the peak intensity (A cm^{-2}), C is the electroactive substance concentration at the electrode surface (mol cm^{-3}), D is electroactive substance diffusion coefficient (cm^2 s^{-1}) and v is the potential sweep rate (V s^{-1}).

At 1083 K, U(IV) diffusion coefficient is equal to $1.7 \pm 0.1 \times 10^{-5}$ cm^2/s and U(III) diffusion coefficient is equal to $2.4 \pm 0.1 \times 10^{-5}$ cm^2/s. The obtained results are compared with literature results in Table 2.

The results obtained in this work are in good agreement with reference [7]. The limited literature data above indicate a slight fall in D with temperature.

3.4. Electrochemical study on a Ni reactive electrode

Fig. 7 shows a comparison between two cyclic voltammograms plotted on W (grey curve) and on Ni (black curve).

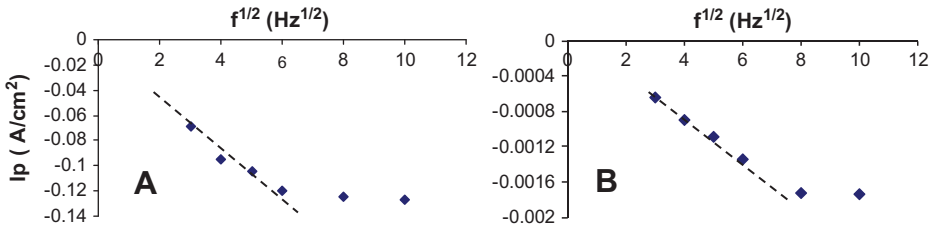

Fig. 5. Dependency of the peak intensity (I_p) in Fig. 4 of the studied U systems versus the square root of frequency ($Hz^{1/2}$).

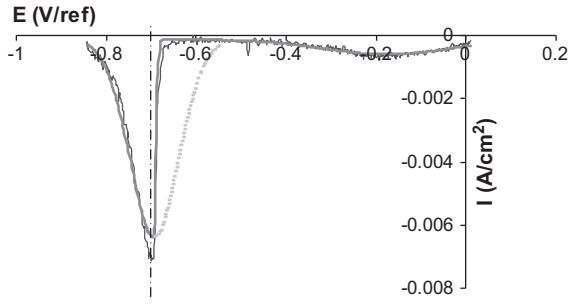

Fig. 6. Comparison of the experimental square wave voltammogram plotted at 9 Hz (black curve) with the deconvoluted signal (grey curve); in dashed gray, the extrapolated part.

Table 2
Comparison of diffusion coefficient determined in this study with literature data.

	This study		[7]		[9]
Media	$LiFCaF_2$		$LiFCaF_2$	LiFNaF	$LiFBeF_2ZrF_4$
Ion	U(IV)	U(III)	U(III)	U(IV)	U(IV)
T (K)	1083	1083	1083	993	773
D (cm^2/s)	1.7×10^{-5}	2.4×10^{-5}	2.2×10^{-5}	1.5×10^{-5}	0.2×10^{-5}

The black curve exhibits a significant peak at −0.16 V, which was not observed on the grey curve. This peak corresponds to the reduction of uranium ions forming intermetallic compounds with the electrode substrate. The depolarisation caused by this phenomenon, i.e. underpotential deposition (UPD), was approximately 0.5 V. The existence of many oxidation waves corresponds to the re-oxidation of the different U_xNi_y compounds (for the U–Ni phase diagram see Fig. 8 [20]) formed during the reduction step.

The U–Ni phase diagram contains 7 intermetallic compounds: two already molten at working temperature (U_6Ni, U_7Ni_9) and 5 solids at working temperature ($U_5Ni_{7+\delta}$, UNi_2, δ, ε and UNi_5).

4. Uranium electrorefining in presence of Gd(III) ions

4.1. Analysis of a melt containing U and Gd ions

Gd(III) ions were introduced to the melt as GdF_3 to simulate the lanthanides formed during fission reactions. 0.5247 g of GdF_3 was added, yielding a concentration of 1.1 wt.%. Fig. 9 shows a cyclic voltammogram plotted using a W electrode in a melt containing both U and Gd ions.

In addition to the previously described U system, a new system attributed to Gd was observed at −1.3 V (C). It has been proven by our previous study [21] that Gd(III) ions are reduced in a single step into Gd metal on an inert electrode in $LiF–CaF_2$ medium. In the present case, the system C was composed of 2 peaks. This discrepancy can be explained by the change of the cathode material due to uranium deposition before the gadolinium reduction.

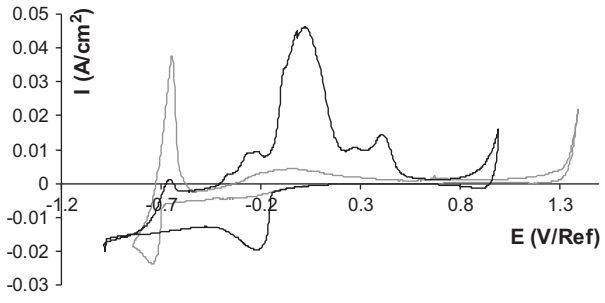

Fig. 7. Comparison of cyclic voltammograms plotted in $LiF–CaF_2–UF_3$ (8.7×10^{-5} mol/kg) at 1083 K; WE: W (grey curve) Ni (black curve), CE: Mo, RE: Pt; v = 100 mV/s.

Fig. 10 shows a comparison of cyclic voltammograms using a Ni working electrode in different melts.

A peak at a potential of −0.16 V was observed on Ni electrode in a melt containing U ions. This peak corresponds to U–Ni alloys formation (cf 3.4) and it was followed by a constant current plateau starting from a potential of −0.38 V. In a melt containing U and Gd ions, the same peak was observed, but in this case the cathodic current steadily increased after this peak. This can be attributed to the reduction of Gd(III) ions forming U–Ni–Gd or Ni–Gd alloys. The mentioned reduction potentials are reported in Fig. 11.

It can be seen that a selective separation of U from Gd on a Ni electrode, required the cathode potential to be kept between −0.16 V and −0.38 V.

4.2. Electrorefining

Electroseparation of uranium from gadolinium was carried out using a nickel plate cathode, while the anode consisted of a tantalum basket filled with uranium metal. During the experiment, U was anodically dissolved and U^{3+} ions were reduced at the cathode, forming U–Ni alloys:

$$\text{Anodic side} \quad U(0) \rightarrow U(III) + 3e^-$$

$$\text{Cathodic side} \quad U(III) + 3e^- \rightarrow U(0) - Ni$$

During the electrolysis, the cathode potential was kept at −0.3 V. As seen in Section 4.1, U(III) should be selectively reduced at this potential, leaving Gd(III) dissolved in the melt at constant concentration. The evolution of cathodic current versus time is reported in Fig. 12.

The increasing deposition current can be explained by an increase of the cathode surface due to electro-formation of U–Ni alloys and also by a shift of the reference potential cathodically. During an electrolysis, the melt composition is always changing and the Pt electrode potential is extremely sensitive to the melt composition [13]. After the electrolysis the electrode was embedded, cut, polished and analysed by SEM–EDS. Fig. 13 shows the electrode SEM analysis.

The following phases were observed:? The bulk of the electrode (Ni), a layer at the electrode surface, composed of the ε phase (see Fig. 8) of composition Ni(78)–U(12) at.% (1) and uranium metal particles detached from the electrode (2) in the salt (3). According to the applied potential, formation of pure U metal was not expected. However, this phenomenon has been already observed in some previous studies, e.g. during underpotential deposition of Sm on Ni and Cu electrodes in the same salt [22,23]. Gd metal was detected neither on the electrode, nor in the salt.

From the previous results, it is possible to calculate the maximum theoretical extraction rate, $\eta = 1 - \frac{a_U^{Finale}}{a_U^{Initiale}}$, of U, where a_U is the activity of U in the melt [24].

$$\Delta E = \frac{RT}{nF} \ln\left(\frac{1}{1-\eta}\right) \tag{8}$$

ΔE, is the difference between U(III) and Gd(III) reduction potential on Ni electrode.

$$\eta = 1 - \exp\left(-\frac{nF}{RT}\Delta E\right) \tag{9}$$

At 1083 K, with ΔE = 0.22 V (cf Fig. 11), η = 99.91%.

These observations demonstrate the feasibility of selective reduction of U(III) ions on the Ni electrode, with good efficiency.

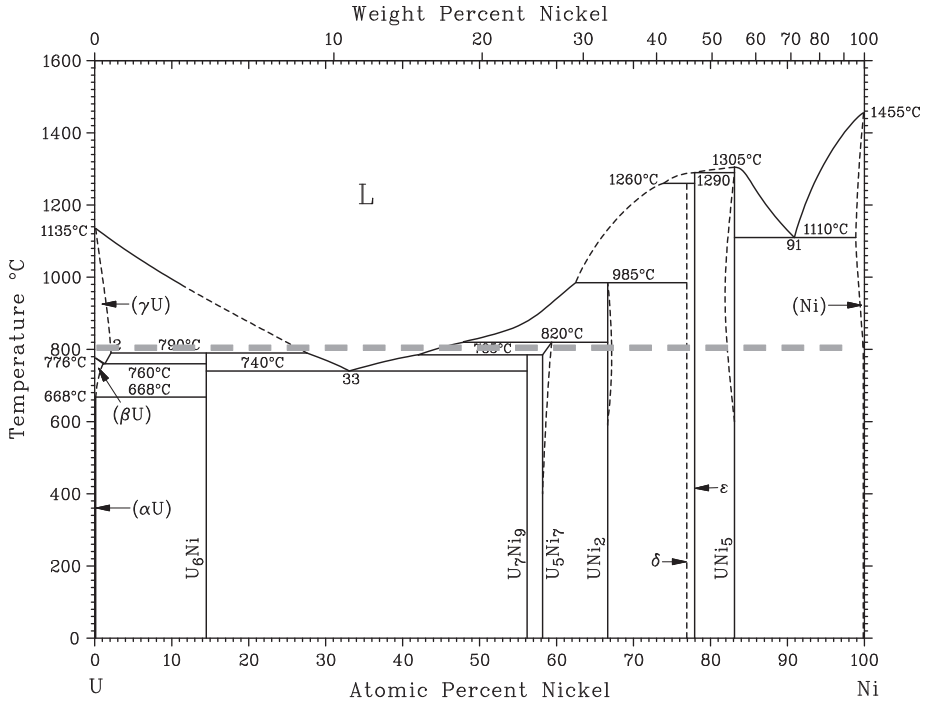

Fig. 8. U–Ni Phase diagram; the dashed grey line corresponds to the working temperature [20].

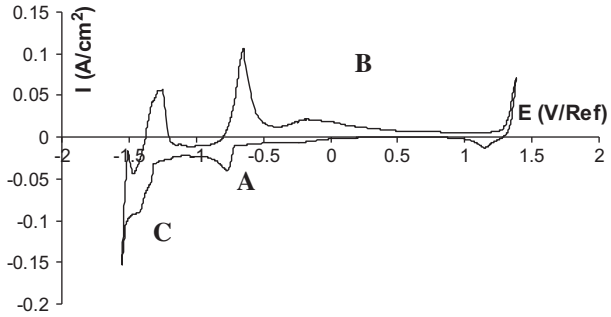

Fig. 9. Cyclic voltammogram plotted in LiF–CaF_2–UF_3 (1.7 wt.%)–GdF_3 (1.1 wt.%) at 1083 K; WE: W, CE: Mo, RE: Pt; v = 100 mV/s.

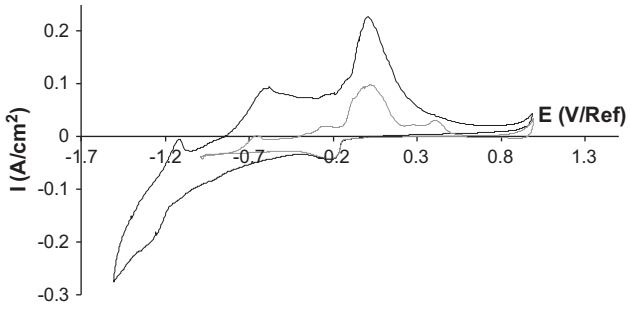

Fig. 10. Comparison of cyclic voltammograms plotted in LiF–CaF_2–UF_3 (1.7 wt.%)–GdF_3 (1.1 wt.%) (black curve) and LiF–CaF_2–UF_3 (1.7 wt.%) (grey curve) at 1083 K; WE: Ni, CE: Mo, RE: Pt; v = 100 mV/s.

5. Summary

The electrochemical behaviour of U(III) has been studied in molten LiF–CaF_2 at 1083 K. The obtained results are in agreement with the literature and show that U(III) is reduced to U metal in one step controlled by diffusion in solution.

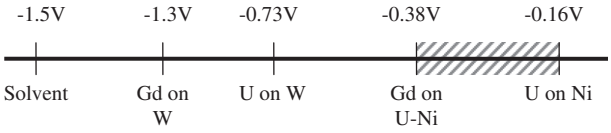

Fig. 11. Potential reduction scale for gadolinium and uranium system on W and Ni electrodes.

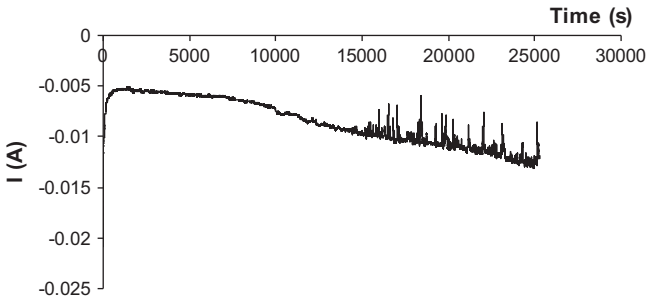

Fig. 12. Variation of the cathodic current versus time during the electrolysis. 215 C have passed through the system during the electrolysis.

Therefore, the present study has also been focused on uranium electrochemical behaviour on nickel, which has been selected as a possible candidate for a solid reactive electrode for electrorefining process for recovery of actinides from spent fuel in molten fluorides.

The phenomenon known as depolarisation has been observed on Ni electrode. A study of a melt containing U and Gd ions has been carried out and shows that selective separation of uranium is possible on a Ni electrode in an appropriate potential range. Electrorefining of a uranium plate in a melt containing Gd(III) ions has been performed. This is the first step to prove the feasibility of

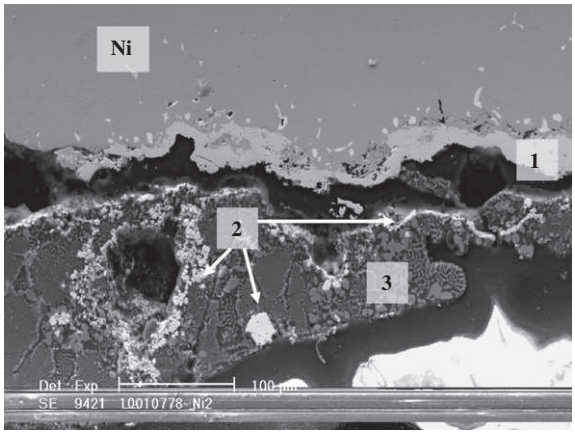

Fig. 13. SEM analysis of the Ni cathode after a 215 C electrolysis in LiF–CaF_2–UF_3 (1.7 wt.%)–GdF_3 (1.1 wt.%).

selective reduction of U(0) on Ni electrode. Although the used parameters in this experiment were different from the real conditions expected for the process (i.e. the concentration of Gd(III) remained constant during the electrolysis), this experiment indicates the potential applicability of the method for irradiated fuel.

Acknowledgements

The authors wish to thank M. Cardinale for ICP–MS analysis as well as M. Ougier and A. Rodrigues for experimental support. This work was carried out with European Commission financial support in the 7th Framework programme, under the Contract 211267 "ACSEPT".

References

[1] Actinide and Fission Product Partitioning and Transmutation – Status and Assessment report, OECD-NEA, 1999. <http://www.nea.fr>.
[2] L. Cassayre et al., J. Nucl. Mater. 360 (2007) 49–57.
[3] P. Souček et al., Radiochim. Acta 96 (2008) 315–322.
[4] M. Iizuka et al., J. Nucl. Mater. 359 (1–2) (2006) 102–113.
[5] M. Iizuka et al., J. Nucl. Sci. Technol. 44 (5) (2007) 801–813.
[6] J. Lacquement et al., J. Fluorine Chem. 130 (2009) 18–21.
[7] C. Hamel et al., Electrochim. Acta 52 (2007) 3995–4003.
[8] P. Chamelot et al., Electrochim. Acta 55 (2010) 4758–4764.
[9] G. Mamantov et al., Anal. Chem. 38 (1966) 1494.
[10] Afonichkin et al., J. Nucl. Mater. 419 (1–3) (2011) 347.
[11] Straka et al., J. Radioanal. Nucl. Chem. 284 (1) (2010) 245.
[12] Clayton et al., J. Electrochem. Soc. 121 (1) (1974) 86.
[13] A.D. Graves, Nature 20 (8) (1965) 481.
[14] A.J. Bard, Electrochemical Methods, Fundamentals and Applications, John Wiley & Sons, 1980 (Chapter 6).
[15] P. Chamelot et al., Electrochim. Acta 39 (1994) 2571.
[16] P. Chamelot et al., Electrochim. Acta 47 (2002) 3423.
[17] B. Trémillon, Electrochimie analytique et réactions en solution, tome 2, Masson, 1993 (Chapter 9).
[18] T. Berzins et al., J. Am. Chem. Soc. 75 (1953) 555.
[19] T. Store et al., J. Appl. Electrochem. 30 (2000) 1351.
[20] T.B. Massalski (Ed.), Binary Alloy Phase Diagrams, second ed., ASM International, 1990 (available on CD-ROM).
[21] C. Nourry et al., Electrochim. Acta 53 (5) (2008) 2650–2655.
[22] P. Taxil et al., J. Fluorine Chem. 130 (2009) 94–101.
[23] C. Nourry, Thesis, Université de Toulouse, France, 2007.
[24] P. Chamelot et al., J. Nucl. Mater. 360 (2007) 64–74.